

A Novel Missense Mutation of Wilms' Tumor 1 Causes Autosomal Dominant FSGS

Gentzon Hall,^{*,†‡} Rasheed A. Gbadegesin,^{*,‡§} Peter Lavin,^{||} Guanghong Wu,[‡] Yangfan Liu,^{||**} Edwin C. Oh,^{||**} Liming Wang,^{*} Robert F. Spurney,^{*,†} Jason Eckel,^{*,†} Thomas Lindsey,[‡] Alison Homstad,[‡] Andrew F. Malone,^{*,†‡} Paul J. Phelan,^{*,†‡} Andrey Shaw,^{††} David N. Howell,^{†‡} Peter J. Conlon,^{||} Nicholas Katsanis,^{†||**} and Michelle P. Winn^{*,†‡}

^{*}Division of Nephrology, Departments of [†]Medicine, [§]Pediatrics, ^{‡‡}Pathology, and ^{||}Cell Biology, [‡]Duke Molecular Physiology Institute, ^{**}Center for Human Disease Modeling, Duke University Medical Center, Durham, North Carolina; ^{††}Department of Pathology and Immunology, Washington University School of Medicine in St. Louis, St. Louis, Missouri; and ^{||}Department of Transplant, Urology and Nephrology, Beaumont Hospital, Dublin, Ireland

ABSTRACT

FSGS is a clinical disorder characterized by focal scarring of the glomerular capillary tuft, podocyte injury, and nephrotic syndrome. Although idiopathic forms of FSGS predominate, recent insights into the molecular and genetic causes of FSGS have enhanced our understanding of disease pathogenesis. Here, we report a novel missense mutation of the transcriptional regulator Wilms' Tumor 1 (WT1) as the cause of nonsyndromic, autosomal dominant FSGS in two Northern European kindreds from the United States. We performed sequential genome-wide linkage analysis and whole-exome sequencing to evaluate participants from family DUK6524. Subsequently, whole-exome sequencing and direct sequencing were performed on proband DNA from family DUK6975. We identified multiple suggestive loci on chromosomes 6, 11, and 13 in family DUK6524 and identified a segregating missense mutation (R458Q) in WT1 isoform D as the cause of FSGS in this family. The identical mutation was found in family DUK6975. The R458Q mutation was not found in 1600 control chromosomes and was predicted as damaging by *in silico* simulation. We depleted *wt1a* in zebrafish embryos and observed glomerular injury and filtration defects, both of which were rescued with wild-type but not mutant human WT1D mRNA. Finally, we explored the subcellular mechanism of the mutation *in vitro*. WT1^{R458Q} overexpression significantly downregulated nephrin and synaptopodin expression, promoted apoptosis in HEK293 cells and impaired focal contact formation in podocytes. Taken together, these data suggest that the WT1^{R458Q} mutation alters the regulation of podocyte homeostasis and causes nonsyndromic FSGS.

J Am Soc Nephrol 26: ●●●–●●●, 2014. doi: 10.1681/ASN.2013101053

FSGS is a heterogeneous disorder characterized by focal scarring of the glomerular capillary tuft, podocyte injury, nephrotic syndrome, and rapid progression to end stage kidney disease (ESKD). FSGS remains one of the leading causes of ESKD worldwide and accounts for 20%–25% of all incident cases of ESKD in the United States.^{1,2} An incomplete understanding of the pathophysiologic mechanisms of this heterogeneous disorder has resulted in a limited number of variably effective therapeutic options. Recent insights into the molecular and genetic mechanisms of hereditary FSGS have

informed our understanding of the pathobiology of FSGS and highlighted podocyte injury as central to disease pathogenesis. The discovery of mutations

Received October 8, 2013. Accepted June 29, 2014.

Published online ahead of print. Publication date available at www.jasn.org.

Correspondence: Dr. Michelle P. Winn, Center for Human Genetics, Duke University Medical Center, Duke Box 2903, Durham, NC 27710. Email: michelle.winn@duke.edu

Copyright © 2014 by the American Society of Nephrology

in a growing number of genes encoding podocyte proteins have demonstrated that derangements of podocyte structural integrity and function are central features in the development of FSGS.^{3–8} Mutations affecting the transcriptional regulation of podocyte structural proteins have also been identified. In particular, various mutations of the Wilms' Tumor 1 (*WT1*) gene have been identified as causes of syndromic hereditary FSGS and diffuse mesangial sclerosis (DMS).⁹ Mutations in *WT1* are typically heterozygous and are usually germline or *de novo*, although occasional parent-to-child transmission has been reported.¹⁰ *WT1* encodes a zinc finger DNA-binding protein that is critical for kidney, urinary tract, and gonadal development.¹¹ Mutations within the C-terminal zinc finger domains encoded by exons 8 and 9 have been shown to impair the transactivating functions of this podocyte-specific nuclear transcription factor resulting in significant alterations in gene expression of essential slit diaphragm components such as nephrin, podocin, and podocalyxin.^{12–17} Renal phenotypes associated with *WT1* mutations include Wilms' tumor as a component of WAGR syndrome (Wilms' tumor, aniridia, genitourinary anomalies, and mental retardation), Denys–Drash syndrome (DDS; Wilms' tumor, male pseudohermaphroditism, and early onset nephrotic syndrome with DMS histology), Frasier syndrome (male pseudohermaphroditism, nephrotic syndrome with FSGS histology, and development of gonadoblastoma), and in some cases nonsyndromic, early onset nephrotic syndrome characterized by DMS histology.^{11,12,18–21} To our knowledge, only one case of nonsyndromic, hereditary FSGS due to *WT1* mutation, without functional validation, has been reported.¹⁰ Here, we report a novel missense mutation in exon 9 of *WT1D* (R458Q; transcript ENST00000332351) as a cause of familial FSGS in two multigenerational families of Northern European descent. We demonstrate that depletion of *wt1a* in zebrafish results in defects in podocyte development coupled with glomerular injury and nephrosis that is rescued by coexpression of wild-type (WT) human *WT1D* mRNA, but not *WT1D*^{R458Q} mRNA. The failure of *WT1D*^{R458Q} to rescue the *wt1a* morpholino (MO) phenotype suggests a loss-of-function mutation. Given the established role of WT1 in podocyte gene regulation,^{13,14} we overexpressed WT1^{WT} and WT1^{R458Q} in human embryonic kidney 293 (HEK293) cells and observed a reduction of nephrin and synaptopodin expression and increased apoptosis in WT1^{R458Q}-overexpressing cells. Furthermore, we demonstrate WT1-dependent podocyte synaptopodin expression and impaired focal contact formation and wound healing in WT1^{R458Q}-overexpressing podocytes. In summary, these data provide evidence of a novel mutation within the third zinc finger domain of WT1 (WT1^{R458Q}) that causes autosomal dominant FSGS. We also provide novel evidence for the role of WT1 in the transcriptional regulation of synaptopodin gene expression. Finally, we demonstrate the deleterious effects of the WT1^{R458Q} mutation on cell viability and function *in vitro* and provide *in vivo* evidence of the loss-of-function effect of the WT1^{R458Q} mutation.

RESULTS

Clinical Data and Linkage Analyses

Family DUK6524 is a 5-generation, 88-member kindred from the United States. Eight affected individuals have biopsies diagnostic of or consistent with FSGS (Figure 1A). In Figure 1, B and B', representative periodic acid–Schiff and Masson trichrome–stained sections of kidney biopsy material from the proband demonstrate segmental sclerosis of glomeruli characteristic of FSGS. Both male and female individuals are affected in at least four generations and there is male-to-male transmission consistent with an autosomal dominant pattern of inheritance (Figure 1A, sex has been deidentified to protect the privacy of individuals). A summary of relevant phenotypic information in six affected individuals is shown in Table 1. In brief, the age of onset of ESKD occurred between ages 17 and 33 years. Three of the six affected family members received kidney transplants without recurrence of disease. Disease-causing mutations in *ACTN4*, transient receptor potential canonical isotype 6 (*TRPC6*), and *INF2* were not found in any of the affected individuals. Genome-wide linkage analysis revealed two-point log of the odds of linkage (LOD) scores of >1.6 on chromosomes 6p (minimal candidate region [MCR]=4.7 MB), 11p (MCR=9.4 MB), and 13p (MCR=21.7 MB) (Figure 2, A and B).

Whole-Exome Sequencing

The DNA from the proband was subjected to whole-exome sequencing using the Illumina TruSeq platform. On average, the genomic coverage was 52×. After excluding variants with minor allele frequency >1%, 1280 novel variants were identified. The following parameters were used to determine the disease-causing mutation: (1) all variants found in our database of 1600 normal control chromosomes were removed; (2) variants that were in the dbSNP (<http://www.ncbi.nlm.nih.gov/projects/SNP/>) and 1000 Genome Project (<http://www.1000genomes.org/>) databases were removed; (3) all synonymous variants were removed; and (4) all intronic variants were removed except those variants that were in obligatory splice sites, were in promoter regions, or were within 25–50 bases of the intron/exon boundaries.^{3,22–25} After applying these parameters, there were 187 potential disease-causing variants from the whole-exome data. All of these potential variants were confirmed by Sanger sequencing. The chromosome 11p peak area contains the *WT1* gene (Supplemental Figure 1). A nonsynonymous heterozygous missense change in exon 9 (1327G>A) resulting in an R458Q was identified in *WT1D* in the proband (Figure 2C). An identical change was identified by whole-exome sequencing and confirmed with direct sequencing in a second family with autosomal dominant FSGS (DUK6975) in our cohort (Figure 2C). The abbreviated pedigree for family DUK6975 is shown in Supplemental Figure 2. The R458Q variant (WT1^{R458Q}) was the only variant that segregates with disease in the family. The variant is absent from >1600 control chromosomes and is absent from the

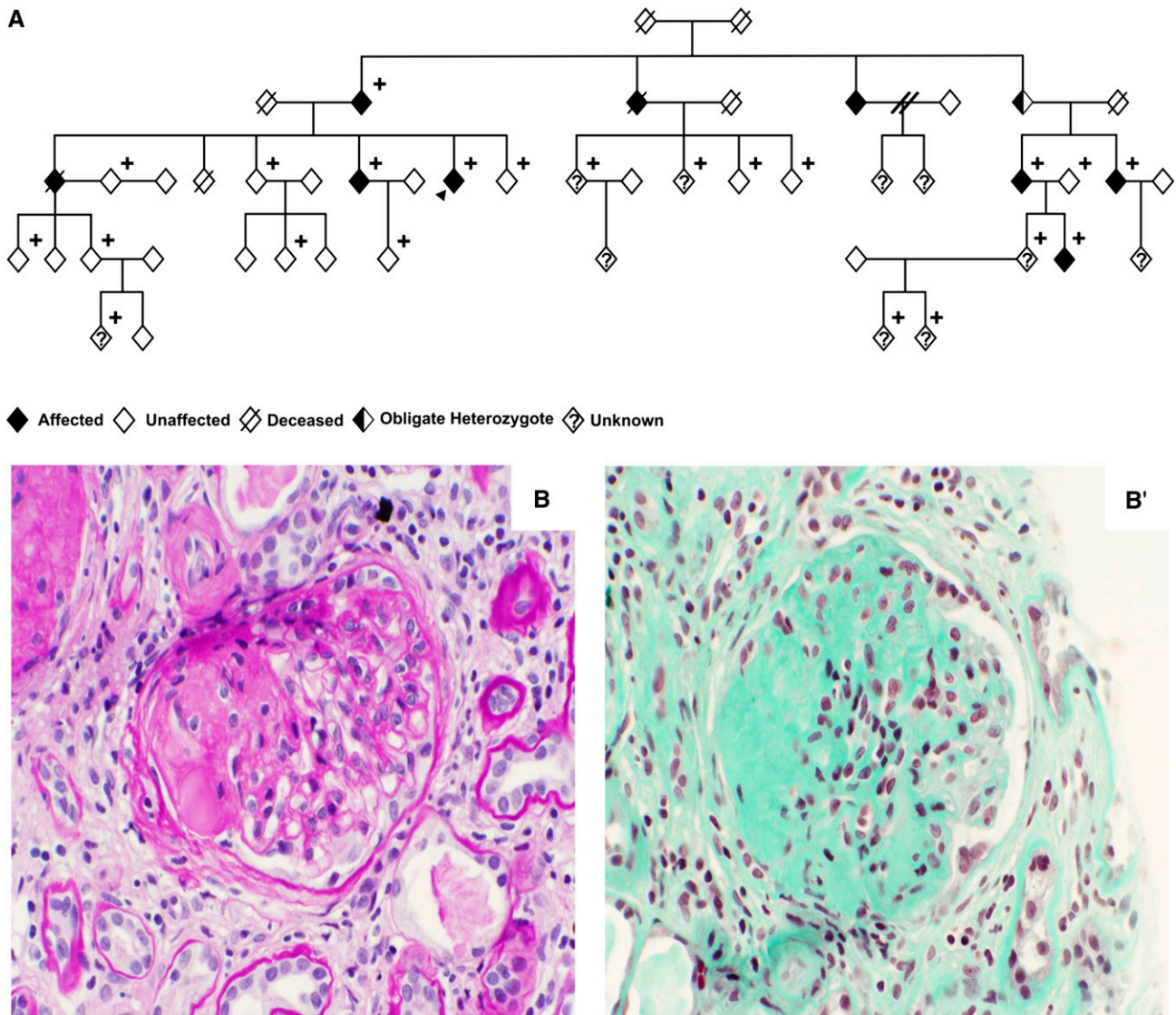


Figure 1. Family DUK6524 pedigree and representative kidney biopsy. (A) Pedigree of family DUK6524, an 88-member kindred from the United States with 9 affected family members with biopsies consistent with a diagnosis of FSGS. (B and B') Proband renal biopsy specimen. Representative kidney biopsy histology from the proband of family DUK6524 showing typical FSGS lesions by light microscopy.

Table 1. Clinical characteristics

| Individual Number | Age at Diagnosis (yr) | Sex | Urinary Protein (g/24 h) | Renal Biopsy Findings | Age at ESKD (yr) | Transplant/Recurrence |
|-------------------|-----------------------|--------|--------------------------|-----------------------|------------------|-----------------------|
| 01 | 30 | Female | NA | FSGS | Unknown | Yes/no |
| 101 | 24 | Male | 7.3 | FSGS | 27 | Yes/no |
| 113 | 28 | Male | 1.0 | FSGS | 33 | Yes/no |
| 122 | Unknown | Male | 1.0 | NA | Unknown | NA/NA |
| 1005 | Unknown | Male | U | Unknown | Unknown | NA/NA |
| 9014 | 16 | Male | 1 | FSGS | 17 | NA/NA |

Family 6524 is an 88-member kindred from the United States with 9 affected individuals. All available biopsies were diagnostic of or consistent with FSGS. Three family members are known to have received renal allografts without recurrence of disease. N/A, not applicable.

publicly available 1000 Genome Project data set. This is a sufficient number of controls for a rare Mendelian disease, because a minimum of 350 is needed for 95% power to detect

1% polymorphism frequency.²⁶ The mutation is conserved in evolution to stickleback (Figure 2E). *In silico* modeling with PolyPhen revealed that the variant is damaging with a

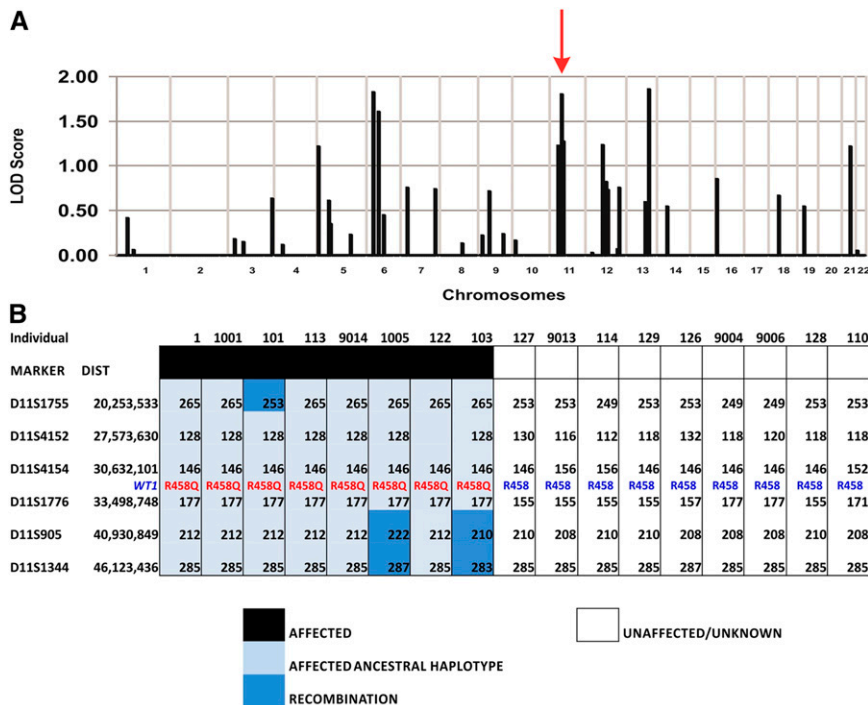


Figure 2. *WT1* mutation in two kindreds with autosomal dominant FSGS. (A) Genome-wide linkage analysis using the Illumina Infinium II HumanLinkage-12 genotyping beadchip assay yielded suggestive LOD scores of >1.6 on chromosomes 6, 11, and 13 in family DUK6524. Chromosome numbers are shown on the x axis and LOD scores are on the y axis. *WT1* is located in the chromosome 11p peak (red arrow). (B) Haplotype analysis for region of interest on chromosome 11, with the MCR spanning a physical distance of 9.4 MB delimited by microsatellite markers D11S4152–D11S1176. (C) An identical missense heterozygous mutation in exon 9 1327G \rightarrow A R458Q found in exon 9 of *WT1* in families DUK6524 and DUK6975. WT control sequence top, mutant sequence below. (D) The R458 residue is conserved in evolution to stickleback.

deleterious score of 0.947; the variant was also predicted to be damaging by SIFT.^{27–29}

Wt1a Deficiency Produces Nephrosis in Zebrafish

The zebrafish embryo has a two-nephron, pronephric kidney with high conservation in patterning and podocyte gene expression profiles compared with mammals. To test the hypothesis that the mutation detected in *WT1D* alters podocyte structure and function during kidney development, we examined the role of *wt1a* in the zebrafish pronephros. *Wt1a* is one of two identified zebrafish orthologs to human *WT1*. Its intracellular functions and localization patterns most closely resemble the characteristics of human *WT1D*. *Wt1a* is a 419-amino-acid zinc finger binding protein found to play an essential role in zebrafish nephron development.^{30,31} Zebrafish embryos staged at the eight-cell stage or earlier were microinjected with a splice-blocking MO against *wt1a* (*wt1a* MO) to suppress the splicing of *wt1a* mRNA.³⁰ In parallel, fluorescein-labeled 70-kD dextran was microinjected into the common

cardinal vein to fill the vascular system of zebrafish embryos; the clearance rate of dextran was used as an established functional expression of filtration efficiency in the zebrafish pronephros.³² At 6 days postfertilization (dpf), we observed pericardial and yolk sac edema in morphant zebrafish larvae relative to control samples (Figure 3, A and B). Rapid dextran clearance was also seen in morphant embryos and the dextran clearance rate was correlated with the presence and severity of edema (Figure 3, E and F). A high dextran clearance rate leads to significantly less fluorescein in the vascular network of the trunk (Figure 3, J and J') and retina (Figure 3N) in morphant relative to control larvae (Figure 3, I, I', and M). Coinjection of human *WT1D*^{WT}—whose protein product shows 71% identity with zebrafish *wt1a* at the amino acid level and whose function, expression, and localization most closely resemble that of *wt1a*—ameliorated the observed phenotypes (Figure 3, C, G, K, K', and O), suggesting these results are gene specific and support the role of *WT1D* in renal filtration.³⁰ To quantify the severity of pronephric filtration leakage, we plotted the percentage of zebrafish larvae with edema and defects in

dextran clearance for each condition (Figure 3Q). Relative to *WT1D*^{WT}, *WT1D*^{R458Q} was unable to rescue the *wt1a* morphant phenotypes (Figure 3, D, H, L, L', and P), suggesting that the R458Q mutation is pathogenic.

To analyze the effects of *WT1D*^{R458Q} mRNA on pronephric kidney development, we next investigated podocyte histology and foot process development by hematoxylin and eosin and transmission electron microscopy. At 6 dpf, we observed a reduction in the size of the kidney in morphant embryos relative to WT samples (Figure 4, A and D); analysis of MO ultrastructure also revealed podocyte foot processes that were broad, flattened and effaced relative to WT samples (Figure 4, C–F). At higher magnification of MO samples, slit diaphragms were not fully articulated and foot processes lacked fine interdigitation (Figure 4, D–F). MO embryos injected with human *WT1D*^{WT} mRNA demonstrated the specificity of mutant phenotypes and resulted in embryos with visible slit diaphragms and well spaced foot processes (Figure 4, G–I); no rescue was evident after injection of the *WT1D*^{R458Q} mRNA into MO-injected embryos (Figure 4,

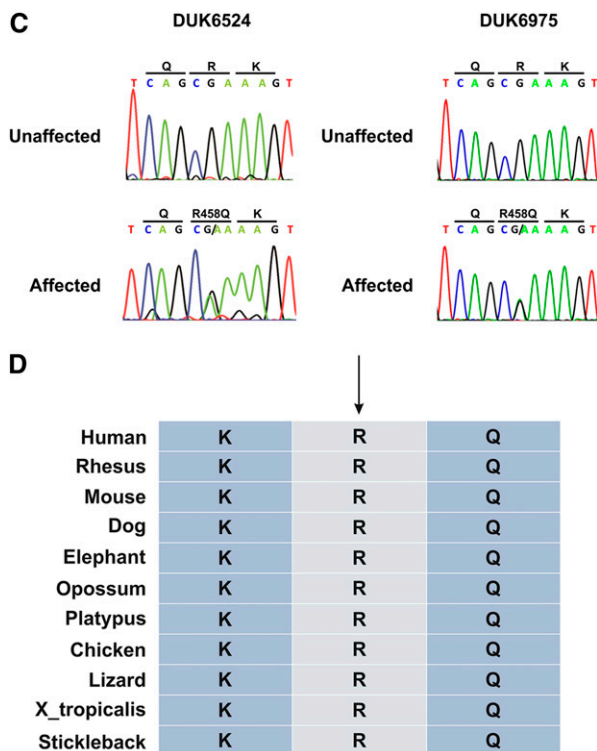


Figure 2. Continued.

J–L). These results support a pathogenic role of the R458Q allele in the development of nonsyndromic FSGS.

WT1^{R458Q} Alters the Regulation of Podocyte Genes

To examine the effects of WT1^{R458Q} on the regulation of key podocyte genes, we used real-time PCR on RNA isolates from WT1^{WT} or WT1^{R458Q}-expressing HEK293 cells. HEK293 cells were selected as the model system for these studies given their amenability to transfection relative to podocytes and because the endogenous expression of multiple slit diaphragm proteins has been previously demonstrated in the line.^{14,33–35} In Figure 5A, we demonstrate that the relative expression of WT1^{WT} and WT1^{R458Q} in transfected HEK293 cells is similar. Because WT1 is recognized as a key regulator of nephrin expression,¹⁴ we evaluated the effect of WT1^{R458Q} expression on mRNA expression of various podocyte slit diaphragm components, including nephrin (*NPISH1*), *TRPC6*, synaptopodin (*SYNPO*), and CD2-associated protein (*CD2AP*) in WT1^{R458Q} and WT1^{WT}-overexpressing HEK293 cells (Figure 5, B and C). There was no significant difference in *TRPC6* or *CD2AP* mRNA expression in WT1^{R458Q} and WT1^{WT}-expressing cells (Figure 5, B and C). By contrast, the expression of *NPISH1* and *SYNPO* was significantly downregulated by 1.6-fold ($P=0.01$) and 2-fold ($P=0.001$) respectively (Figure 5, B and C). These findings support the prior work of Guo *et al.* and Wagner *et al.*, which established WT1 as a regulator of *NPISH1* gene expression,¹⁴ and additionally suggest for the first time that WT1 is a transcriptional regulator of synaptopodin gene activation.

Apoptosis in WT1^{R458Q}-Overexpressing HEK293 Cells

Because of the established role of nephrin in podocyte cell survival signaling,³⁶ we hypothesized that the WT1^{R458Q}-induced decrease in nephrin expression may promote cellular apoptosis. To test this possibility, we conducted FACS analyses for detection of Annexin V staining in WT1^{R458Q}- and WT1^{WT}-overexpressing HEK293 cells. In Figure 5D, WT1^{R458Q}-overexpressing HEK293 cells exhibited a 1.3-fold ($P<0.01$) increase in apoptosis relative to WT1^{WT}-overexpressing cells. These findings demonstrate that WT1^{R458Q}-overexpression promotes cellular apoptosis and may do so *via* a mechanism involving downregulation of nephrin.³⁶

Targeted WT1 Gene Knockdown Attenuates Synaptopodin Expression and Basal Podocyte Motility

WT1 is a known transcriptional activator of nephrin expression in podocytes.³⁷ To evaluate the role of WT1 in podocyte synaptopodin gene expression, we next performed WT1 gene knockdown (KD) in differentiated immortalized human podocytes. WT1 gene KD markedly reduced Synaptopodin expression in podocytes (Figure 6A, $n=2$). In addition, WT1 KD significantly impaired basal podocyte motility by almost 30% (Figure 6, B and C, $n=4$, $P=0.004$). These results demonstrate that WT1 is a transcriptional activator of synaptopodin gene expression and may thereby participate in the regulation of podocyte motility.

Overexpression of WT1^{R458Q} Impairs Focal Contact Assembly in Podocytes

Synaptopodin is known to play an important role in the assembly and maintenance of focal contacts in podocytes through inhibition of Smurf1-mediated polyubiquitination of RhoA.³⁸ Because we established that WT1^{R458Q} overexpression results in decreased synaptopodin expression, we sought to determine the effect of WT1^{R458Q} overexpression on focal contact assembly in podocytes. We confirmed the expression of the integral focal contact protein vasodilator-stimulated phosphoprotein in podocytes under growth-permissive and growth-restrictive conditions (Figure 7A). In WT1^{R458Q}-overexpressing podocytes, the presence of vasodilator-stimulated phosphoprotein in focal contacts is impaired relative to WT1^{WT} or turbo green fluorescent protein (tGFP)-overexpressing cells (Figure 7, $n=2$). These findings suggest that WT1^{R458Q} may exert its deleterious effects on podocyte focal contact assembly through the disruption of Synaptopodin expression.

DISCUSSION

Despite the identification of causal mutations in FSGS, an understanding of the genetic mechanisms in the majority of cases remains elusive. Common to all reports of FSGS is the dysregulation of podocyte homeostasis, suggesting that mechanisms that disrupt this process are germane to the pathogenesis of glomerular damage during the onset and progression of disease. Using linkage analysis and whole-exome sequencing,

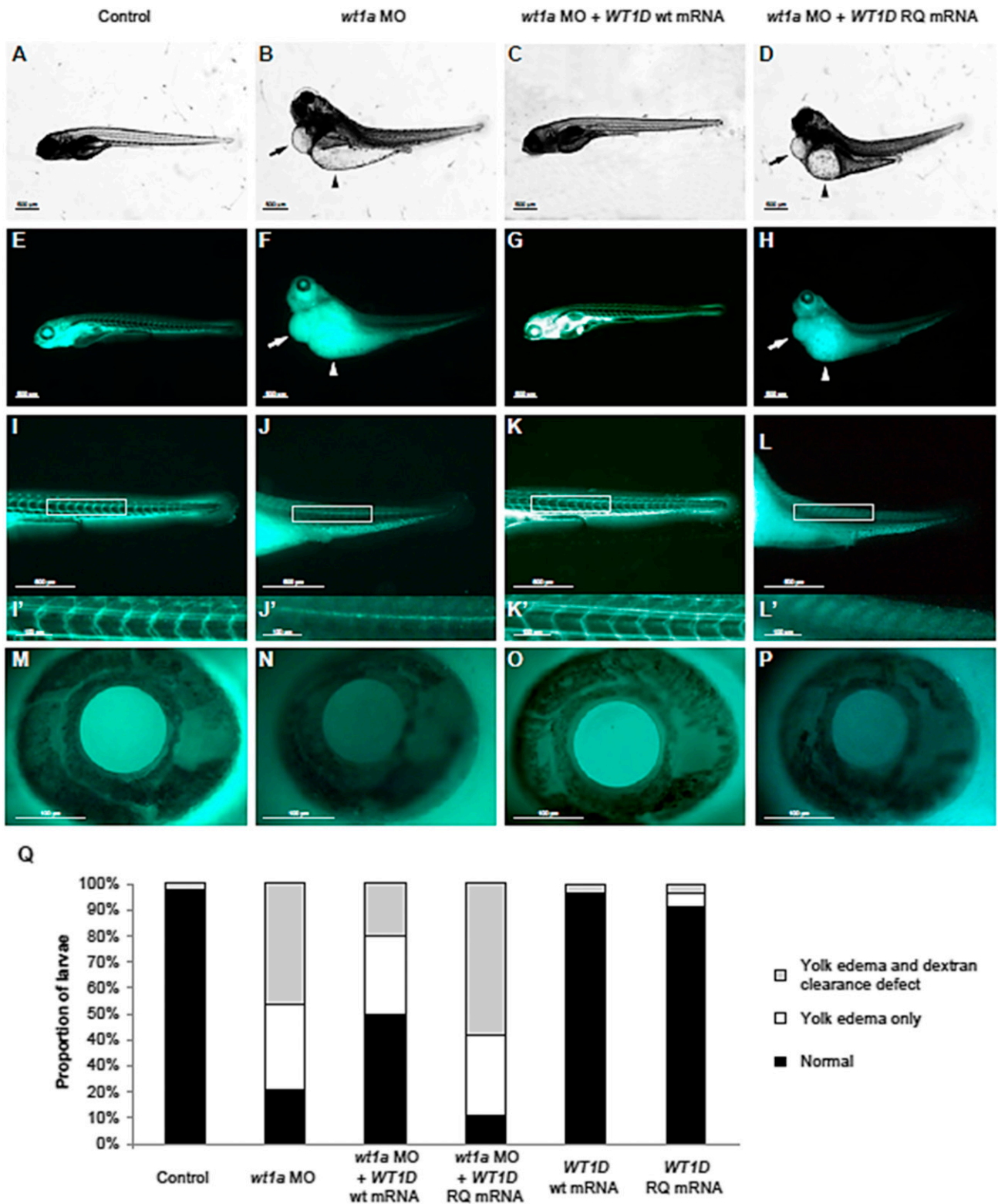


Figure 3. Effect of WT1D^{R458Q} mRNA expression on zebrafish *wt1a*^{-/-} morphant phenotype and glomerular dextran retention. Yolk edema and defects in dextran clearance in *wt1a* zebrafish morphant larvae at 6 dpf can be rescued by human WT1D^{WT} mRNA but not the WT1D^{R458Q} mutant allele. (A–D) Injection of *wt1a* MO (B) results in pericardial (arrow) and yolk sac (arrow head) edema at 6 dpf, which can be rescued by coinjection of human WT1D^{WT} mRNA (C), but not WT1D^{R458Q} mutant mRNA (D). (E–H) Abundant dextran (70 kD) persists in the vascular system of control (E) and WT1D WT mRNA injected larvae (G) at 6 dpf. In MO and WT1D^{R458Q} mRNA

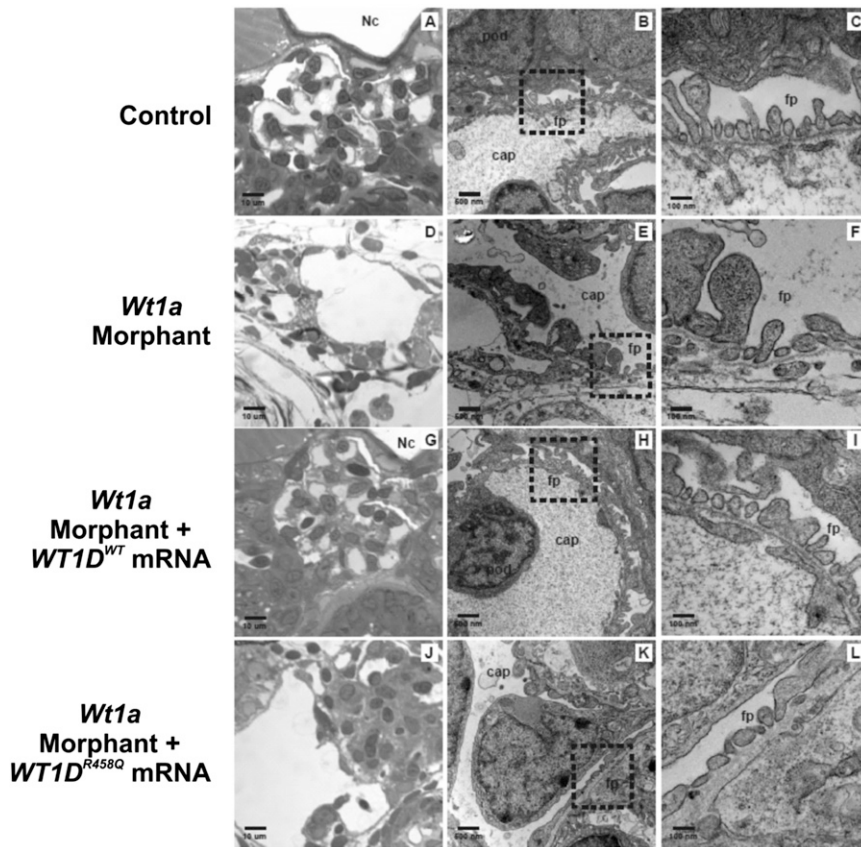


Figure 4. Effect of $WT1D^{R458Q}$ mutation on zebrafish pronephric structure. Histologic aberrations in the pronephric kidney of *wt1a* morphant zebrafish. (A) In control samples, the kidney appears well developed by Lee's stain (A). Ultrastructural analyses reveal podocytes and their foot processes surrounding the capillary lumen along the basement membrane. (B and C) Slit diaphragms are apparent between foot processes. (D–F) In MO samples, the kidney appears irregular (D) and examination of MO ultrastructure shows foot process effacement and lack of fine interdigitation (E and F). (G–I) Phenotypes are specific to the depletion of *wt1a* as injection of human $WT1D^{WT}$ mRNA results in the rescue of mutant kidney phenotypes. Injection of human $WT1D^{R458Q}$ failed to rescue the phenotype of *wt1a* MO suggesting a loss-of-function mutation (J–L). Nc, normal control; fp, foot process; cap, capillary.

we identified a novel mutation in *WT1* that causes a nonsyndromic form of autosomal dominant FSGS. Our *in vivo* and *in vitro* assays demonstrate that *wt1* regulates glomerular morphogenesis and that the mutant R458Q *WT1* allele alters the formation, patterning, and gene expression of podocytes. Given our findings, we recommend the inclusion of *WT1* in future diagnostic platforms that screen for potential causes of autosomal dominant FSGS.

coinjected larvae (H), dextran accumulates in the pericardial and yolk sac edema (arrows and arrowheads). (I–L) The vascular network in the trunk of control (I) and $WT1D^{WT}$ mRNA injected larvae (K) is marked by dextran, whereas the vascular network in the trunk of MO (J) and $WT1D^{R458Q}$ mRNA coinjected larvae (L) is significantly less obvious upon increased clearance of dextran. White boxes delimit images in I'–L'. (M–P) Increased clearance of dextran from the retinal vasculature in MO (N) and $WT1D^{R458Q}$ coinjected larvae (P) results in darker pupils relative to control (M) and $WT1D^{WT}$ mRNA injected larvae (O). (Q) The proportion of zebrafish larvae with yolk edema and dextran clearance defects is plotted for each microinjection condition (MO, mRNA, or both).

Mutations of *WT1* have been associated with syndromic disorders of the renal and urogenital systems such as DDS. DDS results from missense mutations within exons 8 or 9 and produces a classic triad of pseudohermaphroditism, DMS nephropathy, and a predisposition to the development of Wilms' tumor.^{39,40} Notably, the DDS $WT1^{R394V}$ mutation within the third zinc finger binding domain impairs *WT1*-DNA interaction and deleteriously affects the expression of various podocyte genes including nephrin, podocin, and podocalyxin.^{13–17} In 2010, Ratalade *et al.* reported the identification of additional *WT1* gene targets in which expression is affected aberrantly in a murine model of DDS expressing the $WT1^{R394T}$ mutation.¹⁶ Specifically, these authors used gene expression profiling in isolated glomerular preparations from $WT1^{R394T}$ -expressing mice to identify *Scel* and *Sulf1*, two podocyte expressed genes whose downregulation in $WT1^{R394T}$ mutants was strongly associated with the development of the DDS phenotype.¹⁶ Collectively, these findings demonstrate the functional significance of mutations affecting the third zinc finger domain of *WT1* and illustrate the diversity of processes served by *WT1* in the developing renal and urogenital systems.

Our findings reveal that expression of $WT1^{R458Q}$ in HEK cells and differentiated human podocytes produced a number of deleterious effects, including decreased nephrin and synaptopodin mRNA expression, increased apoptosis, and impaired focal contact assembly. Given these findings, we posit that the underlying mechanism

may involve podocyte apoptosis secondary to dysregulation of nephrin-associated survival signaling and podocyte matrix attachment secondary to impaired synaptopodin expression. In support of these hypotheses, Huber *et al.* demonstrated that in HEK293 cells, nephrin and CD2AP interact with the regulatory p85 subunit of PI-3K and that overexpression of nephrin induces AKT-mediated phosphorylation and deactivation of the proapoptotic signaling molecule Bad.³⁶ Subsequently,

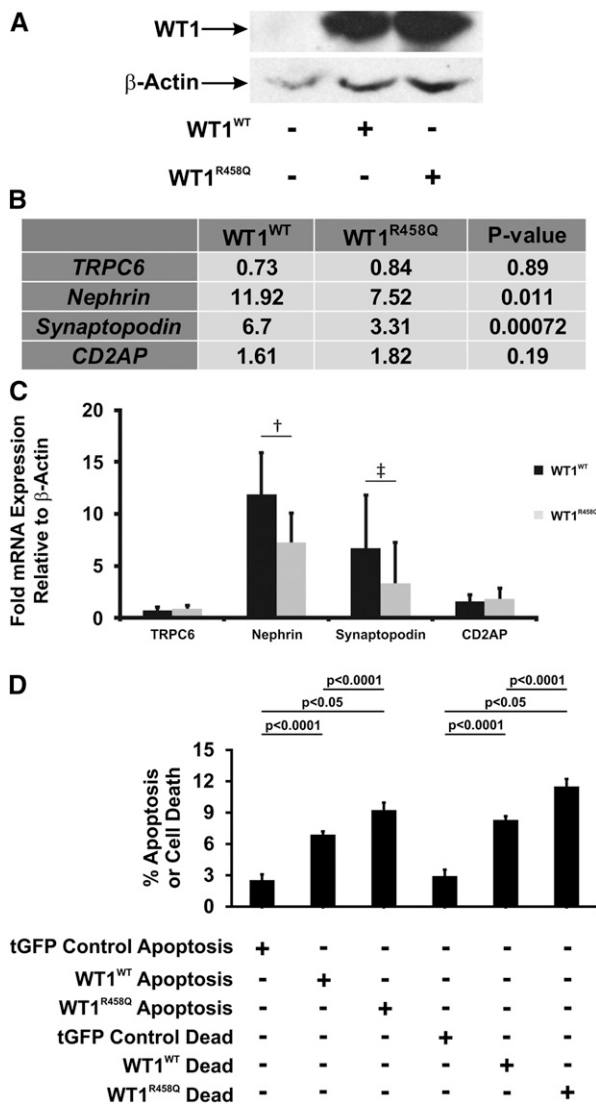


Figure 5. Effect of WT1^{R458Q} mutation on slit diaphragm mRNA expression and apoptosis in HEK293 cells. (A) Representative immunoblot of WT1 expression in transiently transfected HEK293 cells. No significant difference in protein expression observed (quantitation not shown). (B) RT-PCR of mRNA isolates from HEK293 cells transiently transfected with WT1^{WT} or WT1^{R458Q} plasmids. No significant difference between WT1^{WT} and WT1^{R458Q}-expressing cells with respect to TRPC6 and CD2AP expression. HEK cell mRNA expression of nephrin and synaptopodin are significantly reduced in WT1^{R458Q}-expressing cells. (C) Quantitation of relative mRNA expression of TRPC6, CD2AP, nephrin, and synaptopodin in transiently transfected HEK293 cells ([†] $P=0.011$; [‡] $P=0.001$). Results are reported as the mean \pm SEM of three separate experiments. Significance was established at $P<0.05$. (D) Percent apoptosis and cell death in transiently transfected HEK293 cells. Apoptosis and cell death are significantly increased in HEK293 cells expressing WT1^{R458Q} relative to WT1^{WT}-expressing cells. Results are reported as for the mean \pm SEM of 7–15 separate experiments. Significance is established at $P<0.05$.

Guo *et al.* demonstrated that WT1 is a key regulator of nephrin expression in HEK293 cells.¹⁴ It is possible that the increased apoptosis observed in WT1^{R458Q}-expressing HEK cells may be due to disruption of its interaction with p53. Maheswaran *et al.* reported a stabilizing, antiapoptotic interaction with p53, which inhibited apoptosis in Saos-2 osteosarcoma cells.⁴¹ Although this interaction was mapped to the first and second zinc finger regions of WT1, it is possible that the R458Q mutation promotes destabilization and that this interaction leads to increased apoptosis.⁴¹ Alternatively, we do acknowledge that because WT1 is known to be involved in proapoptotic signaling,⁴² the increased apoptosis observed in HEK cells may represent a deleterious gain-of-function effect of the R458Q mutation.

Synaptopodin maintains cytoskeletal integrity, as demonstrated by the work of Yanagida-Asanuma *et al.* in which they demonstrated an essential role for synaptopodin in protection against proteinuria *via* the inhibition of podocyte filopodia formation.⁴³ In addition, Asanuma *et al.* demonstrated that synaptopodin plays an essential role in the formation of focal contacts *via* the inhibition of Smurf1-mediated polyubiquitination of RhoA.³⁸ Specifically, targeted synaptopodin gene knockdown in podocytes promoted derangement of focal contact assembly, podocyte dysmotility, and enhanced RhoA polyubiquitination. Therefore, we recommend that WT1 be included as a cause of nonsyndromic FSGS in the development of future diagnostic platforms.

CONCISE METHODS

Case Ascertainment

Institutional review board approval was obtained from Duke University Medical Center (Durham, NC). Families with FSGS were identified through the International Collaborative Group on Familial FSGS. Inclusion criteria and determination of affection status are as previously reported.⁴⁴ Briefly, inclusion in this analysis required at least one individual with biopsy-proven FSGS and a second family member with FSGS and/or ESKD. Clinical evaluation of these kindreds included a full family history, physical examination, urinalysis with qualitative or quantitative proteinuria, and serum creatinine assay when appropriate. Renal pathology reports and slides were reviewed when available for affected individuals. Individuals were classified as affected, probably affected, or unaffected as follows.

Affected

Individuals were affected if they required dialysis, had undergone renal transplantation, had 2+ to 4+ proteinuria by qualitative urinalysis ≥ 500 mg/24 h on quantitative urinalysis, or had a renal biopsy demonstrating FSGS without evidence of other systemic diseases known to cause FSGS or chronic renal failure.

Probably Affected

Participants were classified as probably affected if they had trace to 1+ proteinuria on qualitative urinalysis. These individuals were categorized as unknown in the linkage analysis.

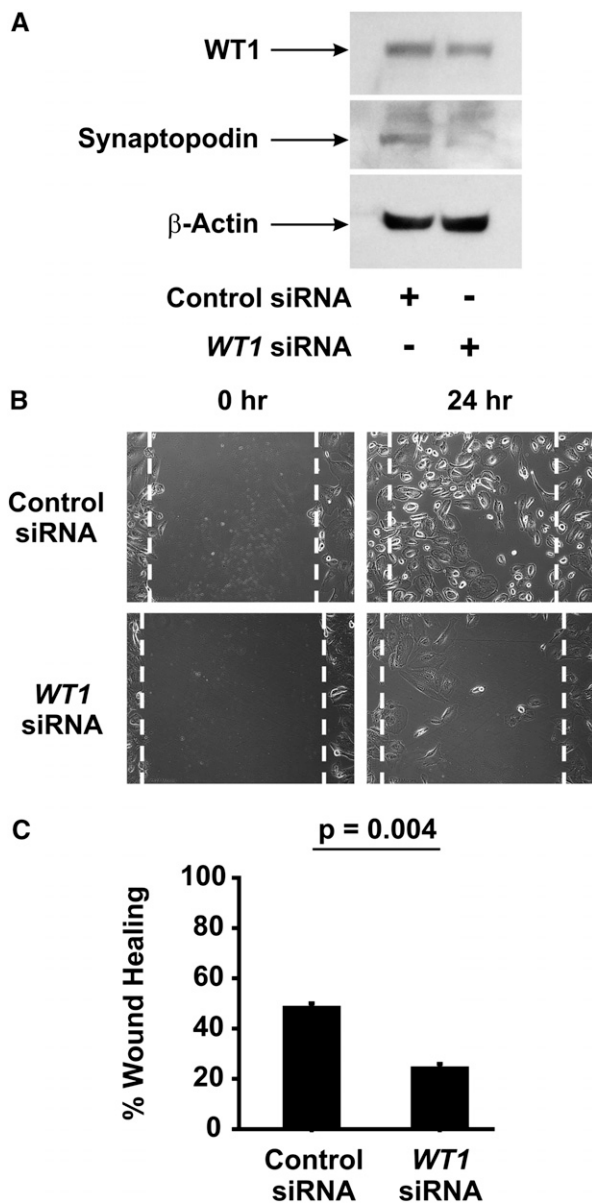


Figure 6. Targeted *WT1* gene knockdown attenuates synaptopodin expression and basal podocyte motility. (A) Representative immunoblot of *WT1* KD in podocytes ($n=2$). (B) Wound healing in *WT1* KD podocytes. Note the significant reduction in basal podocyte motility in *WT1* KD podocytes relative to controls ($P=0.004$). (C) Quantitation of podocyte wound healing. Data are expressed as the percent wound healing, which represents the percent difference in wound area remaining after 24 hours. Results are reported as the mean \pm SEM of four separate experiments. Significance is established at $P<0.05$.

Unaffected

Individuals who had no detectable proteinuria on qualitative urinalysis and were unrelated married-in spouses were classified as unaffected. We excluded mutation in known autosomal dominant FSGS genes (*ACTN4*, *TRPC6*, and *INF2*) in all of the affected individuals.

Genotyping and Linkage Analyses

DNA Isolation and Genotyping

Genomic DNA was isolated from peripheral blood through the Center for Human Genetics at the Duke University Medical Center using PureGene. Fluorescence genotyping was carried out as described⁴⁴ with 135 prelabeled Hex and Fam multiplex primer sets, comprising 351 microsatellite markers, which provided an average spacing of 10 cM across the genome. A Hitachi FMBIOII was used for detection; data were processed using Bio Image and databased using Pedigene.⁴⁴

Linkage Analyses

Two-point and multipoint LOD scores were calculated using VITESSE.⁴⁵ A LOD score of ≥ 3.0 is considered significant evidence for linkage and ≤ -2.0 is significant evidence for exclusion of linkage to the region. Values in between these are inconclusive and additional data are needed before a conclusion can be reached. For two-point LOD scores ≥ 3.0 , a 1-LOD-unit-down support interval was calculated as an approximation to a 95% confidence interval.⁴⁶ Marker allele frequencies were calculated using approximately 100 chromosomes from unrelated, ethnically matched controls. The marker allele/control frequencies did not differ substantially from those calculated from the unrelated spouses in the family. In addition, a conservative low-penetrance “affected-only” analysis was performed to ensure that results obtained were not due to asymptomatic individuals who were nonpenetrant carriers of the FSGS gene. Map distances

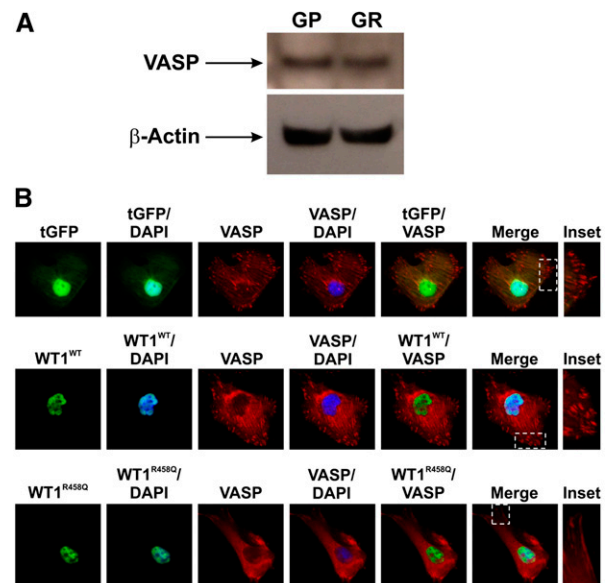


Figure 7. Overexpression of *WT1*^{R458Q} impairs focal contact assembly in podocytes. (A) Expression of vasodilator-stimulated phosphoprotein (VASP) is confirmed by immunoblot analysis in immortalized podocytes under growth-permissive and growth-restrictive conditions. (B) Representative images of immortalized human podocytes overexpressing *WT1*^{WT} or *WT1*^{R458Q} immunostained for the focal contact protein VASP. Note the impaired formation focal contacts in *WT1*^{R458Q}-overexpressing cells (inset) relative to those seen in tGFP-overexpressing controls or *WT1*^{WT}-overexpressing cells.

for the marker loci were obtained from published data (<http://www.gdb.org/>).

Haplotype Analyses

Haplotype analysis was performed as previously described⁴⁷ to identify critical recombination events. Briefly, haplotype analysis was carried out *via* visual inspection, assigning the most likely linkage phase by minimizing the number of recombinants within a pedigree. A candidate interval was considered excluded when two affected individuals within a pedigree inherited different haplotypes from a common affected ancestor. Finally, genetic heterogeneity was evaluated by using the admixture test as implemented in HOMOG.⁴⁶

Sequencing

Whole-Exome Sequencing

Whole-exome sequencing was performed on the proband using standard protocols. We used the Agilent All Exon 50MB kit and sequenced to 78.3× coverage using one lane of a HiSeq 2000 sequencer. Reads were aligned to the Human Reference genome (HG18) using the BWA software. Any homozygous variants with <10× coverage were also Sanger sequenced to eliminate false negative results. Single nucleotide variants were called using SAM tools. The variants were annotated to Ensembl (<http://useast.ensembl.org/index.html>) 50_361 using SequenceVariantAnalyzer and were analyzed using the ATAV software.

Sanger Sequencing

All of the potential disease-causing variants that were identified genome wide were confirmed by Sanger sequencing. Briefly, both strands of all of the variants were sequenced using exon flanking primers. In addition, both strands of all the coding exons of *WT1* were sequenced in 100 families with FSGS using the same method. All sequences were analyzed with Sequencher software (Gene Codes Corp., Ann Arbor, MI).

In Silico Prediction of the Effect of Amino Acid Substitution

The R458Q variant in *WT1* was entered into PolyPhen 2 software to examine the predicted damaging effect of the amino acid substitution to the function of *WT1*. The HumVar-trained version was used, which is optimal for Mendelian disorders because it distinguishes mutations with drastic effects from all the remaining human variation, including abundant mildly deleterious alleles. PolyPhen-2 calculates a naïve Bayes posterior probability that any mutation is damaging and this is represented with a score ranging from 0 to 1. A mutation was also appraised qualitatively, as benign, possibly damaging, or probably damaging based on the model's false positive rate.²⁷

HEK293 Culture and mRNA Extraction

HEK293 cultures were established as previously described.³ Total RNA was manually extracted from HEK293 cells using an RNeasy Mini kit (Qiagen, Valencia, CA). Subsequently, 0.5 µg of total RNA was reverse transcribed into cDNA utilizing the RT system (Promega Corporation, Madison, WI) with oligo(dT) primers, according to the manufacturer's protocol. The cDNA was diluted 2.5-fold for the real-time PCR reaction. Quantification of mRNA by real-time PCR was

performed using the ABI 7900 HT system (Applied Biosystems, Foster City, CA). PCR reactions for *β-Actin* and *WT1*, *TRPC6*, *NPHS2*, *NPHS1*, *SYNPO*, and *WT1* were performed in a final volume of 10 µl, consisting of 2 µl cDNA, 2.5 µl RNase and DNase free water, 0.5 µl of 20× TaqMan Gene Expression Assays (Table 1), and 5 µl of TaqMan 2× PCR Master Mix (both Applied Biosystems). The target DNA was amplified during 40 cycles of 50°C for 2 minutes, 95°C for 10 minutes, 15 seconds, and 60°C for 1 minute. Each individual experiment was performed three times, in duplicate. Relative expression of the target genes was analyzed by normalizing to the housekeeping gene *β-Actin*.

Immunoblotting

After plasmid transfection, HEK293 cells cultures were washed once with ice-cold PBS. Cells were then harvested in loading buffer (Cell Signaling Technologies, Boston, MA) supplemented with 1 µM calyculin A (EMD Millipore, Billerica, MA) and protease inhibitor cocktail, 1:400 dilution (Sigma-Aldrich). Whole cell extracts were then passed through a 1-ml syringe (BD Biosciences, San Jose, CA) 10 times. Cell lysates were then subjected to SDS-PAGE using NuPAGE 10% Bis-Tris precast gels (Invitrogen) followed by transfer to 0.2-µm pore size polyvinylidene difluoride membrane (EMD Millipore). Membranes were blocked with 1-hour incubation in 5% milk in PBS. Protein immunoblotting was then performed using a mouse monoclonal anti-*WT1* antibody at a dilution of 1:1000 (LifeSpan Biosciences, Seattle, WA) and mouse monoclonal *β-actin* antibody at a concentration of 1:3000 (Sigma-Aldrich). Membranes were then washed once with PBS and incubated for 1 hour with horseradish peroxidase-conjugated goat anti-mouse polyclonal secondary antibody at 1:10,000 dilution (Invitrogen). Immunolabeled proteins were detected using a chemiluminescence detection system (Pierce Biotechnology, Rockford, IL) on Kodak Biomax film (VWR Scientific, Radnor, PA).

Conditionally Immortalized Human Podocyte Culture and Reagents

Conditionally immortalized human podocytes were cultured under growth-permissive conditions at 33°C in RPMI 1640 medium (Gibco, Gaithersburg, MD) supplemented with 10% FBS (Gibco), 1:100 penicillin-streptomycin (Invitrogen, Grand Island, NY), and 5% 100× insulin-transferrin-selenium supplement (Invitrogen). Podocyte differentiation was induced by transfer of cultures to growth-restrictive conditions at 37°C.

Plasmid Construction and Lipid-Based Plasmid Transfection

Plasmids expressing *tGFP-tagged human WT1^{WT}* were purchased from OriGene (Rockville, MD). Site-directed mutagenesis was performed by standard PCR-based methods and plasmid purification was performed using the Qiagen Plasmid Midi Kit. Lipid-based plasmid transfections were performed per manufacturer's protocols using the Lipofectamine LTX with Plus Reagent system (Invitrogen). Briefly, *tGFP* empty vector, *tGFP-WT1^{WT}*, and *tGFP-WT1^{R458Q}* plasmids were combined with Lipofectamine LTX and Plus Reagent per manufacturer's protocol and allowed to incubate at room

temperature for 30 minutes. Growth-restricted conditionally immortalized human podocytes were trypsinized and resuspended after centrifugation in transfection media containing RPMI 1640 supplemented with 10% FBS. Reverse transfection was then performed *via* direct admixture of podocyte cell suspension at a concentration of 4.0×10^5 cells/ml and plasmid DNA-lipid complexes before plating on 100 cm dishes. Cells were then allowed to incubate under growth-restrictive conditions for 48 hours before experimental use. For HEK cell transfections, cells were transfected with tGFP-WT1^{WT}, and 24 hours after transfection, cells were harvested and cell lysates were prepared for immunoblotting or mRNA extraction as previously described.

Immunofluorescence

Conditionally immortalized human podocytes and HEK293 cells were cultured on collagen I-coated coverslips (BD Biosciences) and treated as indicated. Cells were then fixed with 4% paraformaldehyde in PBS (Sigma-Aldrich). Cells were then washed twice with ice-cold PBS before permeabilization with 0.1% Triton X-100 in PBS. Cells were then washed with ice-cold PBS twice and blocked with buffer containing 5% goat serum before incubation with mouse monoclonal WT1 antibody (LifeSpan Biosciences, Seattle, WA), and mouse monoclonal nephrin antibody (Novus Biologicals, Littleton, CO) overnight at 4°C. Cells were then washed with ice-cold PBS and secondary Alexa Flora 488 antibody was applied (Invitrogen) at a concentration of 1:1000 for 1 hour at room temperature. Cells were then washed four times with PBS at room temperature before addition of 4',6-diamidino-2-phenylindole stain at a concentration of 1:10,000 diluted in PBS. Immunofluorescence imaging was performed using a Carl Zeiss AxioImager and the MetaMorph Bioimaging Software.

Apoptosis Assays

HEK293 cells were plated in 12-well tissue culture clusters (Evergreen Scientific, Los Angeles, CA) and transfected with the green fluorescent protein-expressing construct pEGP-N1 (0.4 μ g per well; Clontech Laboratories, Palo Alto, CA) and either wild-type WT1 or mutant WT1 (1.2 μ g per well; Upstate) using Lipofectamine (Invitrogen, Carlsbad, CA) according to the manufacturer's directions. After transfection, HEK293 cells were harvested and apoptosis was detected *via* the presence of Annexin V staining using the BD Pharmingen Annexin V PE kit (San Diego, CA) according to the manufacturer's directions. Quantitation of the apoptotic cells was performed by flow cytometric analysis at the Duke Comprehensive Cancer facility by gating on green fluorescent protein-positive cells. For the Annexin V studies, apoptotic podocytes were differentiated from necrotic cells by counting cells that stained with 7-amino-actinomycin D. Results are expressed as the mean \pm SEM for three experiments with statistical significance established at $P < 0.05$.

Scratch Wound Healing Assay and Reagents

Immortalized podocyte cultures were differentiated under growth-restrictive conditions for 10 days. Cells were then washed once with RPMI 1640 media supplemented with 10% FBS (transfection media). Next, cells were transfected with control or WT1 small interfering RNAs using RNAiMax transfection reagent. Cells were then returned

to growth-restrictive conditions for 3 days before scratch wound creation. Scratch wounds were applied using a 1000- μ l plastic pipette tip. Cell monolayers were then washed once with transfection media after wound creation. Podocytes were then imaged using an EVOS microscope at time 0 hours immediately after wound creation. Cells were then returned to growth-restrictive conditions for 24 hours before final images of wound healing were obtained. Data are expressed as the "percent wound healing," which represents the percent difference in wound area after 24 hours.

In Vivo Analyses

Zebrafish Stocks and Injections

Zebrafish (EK) were grown and mated at 28.5°C, and embryos were kept and handled in embryo medium as previously described.⁴⁸ MO was injected in fertilized eggs in the one- to eight-cell stage using a Picospritzer injection device. The following MO against *wt1a* was designed and ordered from GeneTools (Philomath, OR): 5'-AAAG-TAGTTCCTCACCTTGATTCT-3'. MO injections were carried out with a concentration of 10 ng/nl, with an injection volume of 0.5 nl in 0.1% phenol red). Embryos were monitored for the development of phenotype until 6 dpf. Phenotype was scored relative to the presence of yolk edema and dextran clearance defect.

Eye Assays

Two types of eye assays were performed to assess proteinuria. At 2.5 days after MO injection, remaining chorions were manually removed from all embryos. For one group, cardinal vein injections were performed as described by Hentschel *et al.*³² Briefly, 4.6 nl FITC-labeled 70-kD dextran (Molecular Probes, Eugene, OR) was injected into the common cardinal vein. For this injection, zebrafish were anesthetized in a 0.2 mg/ml Tricaine (ethyl-m-aminobenzoate methanesulfonate, 1% Na₂HPO₄, pH 7.0; Sigma-Aldrich) and positioned on their backs in a 1% agarose injection mold. After the injection, fish were returned to embryo medium, where they quickly regained motility. Fish were anesthetized with Tricaine and sequential images of live fish were generated using a Nikon AZ100 microscope connected to a Nikon DS-Qi1 camera, and images were taken with fixed exposure times and gain using the Nikon NIS-Elements software package.

Statistical Analyses

All data are represented as the mean \pm SEM. Group differences were assessed by the *t* test. Statistical significance was established at $P < 0.05$.

ACKNOWLEDGMENTS

We thank Dr. Elizabeth T. Cirulli, Dr. David B. Goldstein, and the personnel of the Center for Human Genome Variation for assistance with whole-exome sequencing. We also acknowledge the following individuals for the contributions of control samples: Dr. James Burke, Dr. Christine Hulette, Dr. Kathleen Welsh-Bohmer, Dr. Francis J. McMahon, Nirmala Akula, Dr. Julie Hoover-Fong, Dr. Nara L. Sobreira, Dr. David Valle, Dr. M. Chiara Manzini, Dr. Annapurna

Poduri, Dr. Nicole Calakos, Mr. David H. Murdock and The MURDOCK Study Community Registry and Biorepository, Dr. Joseph McEvoy, Dr. Anna Need, Mr. Jordan Silver, Ms. Marlyne Silver, Dr. Eli J. Holtzman, Dr. Gianpiero Cavalleri, Dr. Norman Delanty, Dr. Chantal Depondt, Dr. Sanjay Sisodiya, Dr. William B. Gallentine, Dr. Erin L. Heinzen, Dr. Aatif M. Husain, Ms. Kristen N Linney, Dr. Mohamad A. Mikati, Dr. Rodney A. Radtke, Dr. Saurabh R. Sinha, Ms. Nicole M. Walley, Dr. Deborah Koltai Attix, Ms. Vicki Dixon, Ms. Jill McEvoy, Dr. Vandana Shashi, Dr. Patricia Lugar, Dr. William L. Lowe, Dr. Scott M. Palmer, Dr. Doug Marchuk, Dr. Deborah Levy, Dr. Zvi Farfel, Dr. Doron Lancet, Dr. Elon Pras, Dr. Yong-Hui Jiang, Dr. Qian Zhao, Dr. Joshua Milner, Dr. Demetre Daskalakis, Mr. Arthur Holden, Dr. Elijah Behr, Dr. Robert H. Brown Jr, Dr. Sarah Kerns, and Dr. Harriet Oster. Finally, we thank the personnel of the Center for Human Genetics core facilities and most importantly the family members of the Duke FSGS Project.

M.P.W. is funded by a grant from the National Institutes of Health (NIH) National Institute of Diabetes and Digestive and Kidney Diseases (NIDDK) (5R01-DK074748-06) and is a recipient of a Duke Med Scholars program scholarship. G.H. receives salary support from the NIH/NIDDK (Duke Training Grant in Nephrology 5T32-DK0007731) and is also supported by an NIH/NIDDK Minority Research Supplement (5R01-DK74748-5). R.A.G. is funded by a grant from the NIH/NIDDK (K08-DK082495-03) and the NephCure Foundation. N.K. is funded by a grant from the NIH (P50-DK096415). The sequenced controls used for this study were funded in part by grants from the US Department of Health and Human Services (ARRA 1RC2NS070342-01), the National Institute on Aging (Bryan ADRC NIA P30 AG028377), the National Institute of Mental Health (RC2MH089915), and the National Institute of Allergy and Infectious Diseases (NIAID) (1R56AI098588-01A1). This research was also supported in part by funding from the NIH NIAID Division of Intramural Research.

DISCLOSURES

None.

REFERENCES

1. Dragovic D, Rosenstock JL, Wahl SJ, Panagopoulos G, DeVita MV, Michelis MF: Increasing incidence of focal segmental glomerulosclerosis and an examination of demographic patterns. *Clin Nephrol* 63: 1–7, 2005
2. Hogg R, Middleton J, Vehaskari VM: Focal segmental glomerulosclerosis—epidemiology aspects in children and adults. *Pediatr Nephrol* 22: 183–186, 2007
3. Winn MP, Conlon PJ, Lynn KL, Farrington MK, Creazzo T, Hawkins AF, Daskalakis N, Kwan SY, Ebersviller S, Burchette JL, Pericak-Vance MA, Howell DN, Vance JM, Rosenberg PB: A mutation in the TRPC6 cation channel causes familial focal segmental glomerulosclerosis. *Science* 308: 1801–1804, 2005
4. Boyer O, Benoit G, Gribouval O, Nevo F, Tête MJ, Dantal J, Gilbert-Dussardier B, Touchard G, Karras A, Presne C, Grunfeld JP, Legendre C, Joly D, Rieu P, Mohsin N, Hannedouche T, Moal V, Gubler MC, Broutin I, Mollet G, Antignac C: Mutations in INF2 are a major cause of autosomal dominant focal segmental glomerulosclerosis. *J Am Soc Nephrol* 22: 239–245, 2011
5. Santín S, García-Maset R, Ruiz P, Giménez I, Zamora I, Peña A, Madrid A, Camacho JA, Fraga G, Sánchez-Moreno A, Cobo MA, Bernis C, Ortiz A, de Pablo AL, Pintos G, Justa ML, Hidalgo-Barquero E, Fernández-Llama P, Ballarín J, Ars E, Torra R; FSGS Spanish Study Group: Nephrin mutations cause childhood- and adult-onset focal segmental glomerulosclerosis. *Kidney Int* 76: 1268–1276, 2009
6. Tsukaguchi H, Sudhakar A, Le TC, Nguyen T, Yao J, Schwimmer JA, Schachter AD, Poch E, Abreu PF, Appel GB, Pereira AB, Kalluri R, Pollak MR: NPHS2 mutations in late-onset focal segmental glomerulosclerosis: R229Q is a common disease-associated allele. *J Clin Invest* 110: 1659–1666, 2002
7. Yao J, Le TC, Kos CH, Henderson JM, Allen PG, Denker BM, Pollak MR: Alpha-actinin-4-mediated FSGS: An inherited kidney disease caused by an aggregated and rapidly degraded cytoskeletal protein. *PLoS Biol* 2: e167, 2004
8. Gigante M, Pontrelli P, Montemurno E, Roca L, Aucella F, Penza R, Caridi G, Ranieri E, Ghiggeri GM, Gesualdo L: CD2AP mutations are associated with sporadic nephrotic syndrome and focal segmental glomerulosclerosis (FSGS). *Nephrol Dial Transplant* 24: 1858–1864, 2009
9. Kaltenis P, Schumacher V, Jankauskiene A, Laurinavicius A, Royer-Pokora B: Slow progressive FSGS associated with an F392L WT1 mutation. *Pediatr Nephrol* 19: 353–356, 2004
10. Benetti E, Caridi G, Malaventura C, Dagnino M, Leonardi E, Artifoni L, Ghiggeri GM, Tosatto SC, Murer L: A novel WT1 gene mutation in a three-generation family with progressive isolated focal segmental glomerulosclerosis. *Clin J Am Soc Nephrol* 5: 698–702, 2010
11. Niaudet P, Gubler MC: WT1 and glomerular diseases. *Pediatr Nephrol* 21: 1653–1660, 2006
12. Mucha B, Ozaltin F, Hinkes BG, Hasselbacher K, Ruf RG, Schultheiss M, Hangan D, Hoskins BE, Everding AS, Bogdanovic R, Seeman T, Hoppe B, Hildebrandt F; Members of the APN Study Group: Mutations in the Wilms' tumor 1 gene cause isolated steroid resistant nephrotic syndrome and occur in exons 8 and 9. *Pediatr Res* 59: 325–331, 2006
13. Palmer RE, Kotsianti A, Cadman B, Boyd T, Gerald W, Haber DA: WT1 regulates the expression of the major glomerular podocyte membrane protein Podocalyxin. *Curr Biol* 11: 1805–1809, 2001
14. Guo G, Morrison DJ, Licht JD, Quaggin SE: WT1 activates a glomerular-specific enhancer identified from the human nephrin gene. *J Am Soc Nephrol* 15: 2851–2856, 2004
15. Gao F, Maiti S, Sun G, Ordonez NG, Udtha M, Deng JM, Behringer RR, Huff V: The Wt1+/R394W mouse displays glomerulosclerosis and early-onset renal failure characteristic of human Denys-Drash syndrome. *Mol Cell Biol* 24: 9899–9910, 2004
16. Ratelade J, Arrondel C, Hamard G, Garbay S, Harvey S, Biebuyck N, Schulz H, Hastie N, Pontoglio M, Gubler MC, Antignac C, Heidet L: A murine model of Denys-Drash syndrome reveals novel transcriptional targets of WT1 in podocytes. *Hum Mol Genet* 19: 1–15, 2010
17. Morrison AA, Viney RL, Saleem MA, Lodomery MR: New insights into the function of the Wilms tumor suppressor gene WT1 in podocytes. *Am J Physiol Renal Physiol* 295: F12–F17, 2008
18. Gbadegesin R, Hinkes BG, Hoskins BE, Vlangos CN, Heeringa SF, Liu J, Loirat C, Ozaltin F, Hashmi S, Ulmer F, Cleper R, Ettenger R, Antignac C, Wiggins RC, Zenker M, Hildebrandt F: Mutations in PLCE1 are a major cause of isolated diffuse mesangial sclerosis (IDMS). *Nephrol Dial Transplant* 23: 1291–1297, 2008
19. Chérin G, Vega-Warner V, Schoeb DS, Heeringa SF, Ovunc B, Saisawat P, Cleper R, Ozaltin F, Hildebrandt F; Members of the GPN Study Group: Genotype/phenotype correlation in nephrotic syndrome caused by WT1 mutations. *Clin J Am Soc Nephrol* 5: 1655–1662, 2010
20. Royer-Pokora B, Beier M, Henzler M, Alam R, Schumacher V, Weirich A, Huff V: Twenty-four new cases of WT1 germline mutations and review of the literature: Genotype/phenotype correlations for Wilms tumor development. *Am J Med Genet A* 127A: 249–257, 2004

21. Denamur E, Bocquet N, Mougnot B, Da Silva F, Martinat L, Loirat C, Elion J, Bensman A, Ronco PM: Mother-to-child transmitted WT1 splice-site mutation is responsible for distinct glomerular diseases. *J Am Soc Nephrol* 10: 2219–2223, 1999
22. Shih NY, Li J, Karpitskii V, Nguyen A, Dustin ML, Kanagawa O, Miner JH, Shaw AS: Congenital nephrotic syndrome in mice lacking CD2-associated protein. *Science* 286: 312–315, 1999
23. Boute N, Gribouval O, Roselli S, Benessy F, Lee H, Fuchshuber A, Dahan K, Gubler MC, Niaudet P, Antignac C: NPHS2, encoding the glomerular protein podocin, is mutated in autosomal recessive steroid-resistant nephrotic syndrome. *Nat Genet* 24: 349–354, 2000
24. Kaplan JM, Kim SH, North KN, Rennke H, Correia LA, Tong HQ, Mathis BJ, Rodríguez-Pérez JC, Allen PG, Beggs AH, Pollak MR: Mutations in ACTN4, encoding alpha-actinin-4, cause familial focal segmental glomerulosclerosis. *Nat Genet* 24: 251–256, 2000
25. Hinkes B, Wiggins RC, Gbadegesin R, Vlangos CN, Seelow D, Nürnberg G, Garg P, Verma R, Chaib H, Hoskins BE, Ashraf S, Becker C, Hennies HC, Goyal M, Wharram BL, Schachter AD, Mudumana S, Drummond I, Kerjaschki D, Waldherr R, Dietrich A, Ozaltin F, Bakkaloglu A, Cleper R, Basel-Vanagaite L, Pohl M, Griebel M, Tsygin AN, Soyulu A, Müller D, Sorli CS, Bunney TD, Katan M, Liu J, Attanasio M, O'toole JF, Hasselbacher K, Mucha B, Otto EA, Airik R, Kispert A, Kelley GG, Smrcka AV, Gudermann T, Holzman LB, Nürnberg P, Hildebrandt F: Positional cloning uncovers mutations in PLCE1 responsible for a nephrotic syndrome variant that may be reversible. *Nat Genet* 38: 1397–1405, 2006
26. Collins JS, Schwartz CE: Detecting polymorphisms and mutations in candidate genes. *Am J Hum Genet* 71: 1251–1252, 2002
27. Sunyaev S, Ramensky V, Koch I, Lathe W 3rd, Kondrashov AS, Bork P: Prediction of deleterious human alleles. *Hum Mol Genet* 10: 591–597, 2001
28. Kumar P, Henikoff S, Ng PC: Predicting the effects of coding non-synonymous variants on protein function using the SIFT algorithm. *Nat Protoc* 4: 1073–1081, 2009
29. Sim NL, Kumar P, Hu J, Henikoff S, Schneider G, Ng PC: SIFT web server: Predicting effects of amino acid substitutions on proteins. *Nucleic Acids Res* 40: W452–W457, 2012
30. Perner B, Englert C, Bollig F: The Wilms tumor genes wt1a and wt1b control different steps during formation of the zebrafish pronephros. *Dev Biol* 309: 87–96, 2007
31. Bollig F, Mehringer R, Perner B, Hartung C, Schäfer M, Scharl M, Volff JN, Winkler C, Englert C: Identification and comparative expression analysis of a second wt1 gene in zebrafish. *Dev Dyn* 235: 554–561, 2006
32. Hentschel DM, Mengel M, Boehme L, Liebsch F, Albertin C, Bonventre JV, Haller H, Schiffer M: Rapid screening of glomerular slit diaphragm integrity in larval zebrafish. *Am J Physiol Renal Physiol* 293: F1746–F1750, 2007
33. Zagranichnaya TK, Wu X, Villereal ML: Endogenous TRPC1, TRPC3, and TRPC7 proteins combine to form native store-operated channels in HEK-293 cells. *J Biol Chem* 280: 29559–29569, 2005
34. Sha Y, Huang S, Zhang A, Zhao F, Chen R: Effects of podocin transfection on CD2AP distribution in HEK293 cells. *Front Med China* 2: 35–38, 2008
35. Patrie KM, Drescher AJ, Welihinda A, Mundel P, Margolis B: Interaction of two actin-binding proteins, synaptopodin and alpha-actinin-4, with the tight junction protein MAGI-1. *J Biol Chem* 277: 30183–30190, 2002
36. Huber TB, Hartleben B, Kim J, Schmidts M, Schermer B, Keil A, Egger L, Lecha RL, Borner C, Pavenstädt H, Shaw AS, Walz G, Benzing T: Nephlin and CD2AP associate with phosphoinositide 3-OH kinase and stimulate AKT-dependent signaling. *Mol Cell Biol* 23: 4917–4928, 2003
37. Wagner N, Wagner KD, Xing Y, Scholz H, Schedl A: The major podocyte protein nephrin is transcriptionally activated by the Wilms' tumor suppressor WT1. *J Am Soc Nephrol* 15: 3044–3051, 2004
38. Asanuma K, Yanagida-Asanuma E, Faul C, Tomino Y, Kim K, Mundel P: Synaptopodin orchestrates actin organization and cell motility via regulation of RhoA signalling. *Nat Cell Biol* 8: 485–491, 2006
39. Drash A, Sherman F, Hartmann WH, Blizzard RM: A syndrome of pseudohermaphroditism, Wilms' tumor, hypertension, and degenerative renal disease. *J Pediatr* 76: 585–593, 1970
40. Denys P, Malvaux P, Van Den Berghe H, Tanghe W, Proesmans W: [Association of an anatomo-pathological syndrome of male pseudohermaphroditism, Wilms' tumor, parenchymatous nephropathy and XX/XY mosaicism]. *Arch Fr Pediatr* 24: 729–739, 1967
41. Maheswaran S, Englert C, Bennett P, Heinrich G, Haber DA: The WT1 gene product stabilizes p53 and inhibits p53-mediated apoptosis. *Genes Dev* 9: 2143–2156, 1995
42. Morrison DJ, English MA, Licht JD: WT1 induces apoptosis through transcriptional regulation of the proapoptotic Bcl-2 family member Bak. *Cancer Res* 65: 8174–8182, 2005
43. Yanagida-Asanuma E, Asanuma K, Kim K, Donnelly M, Young Choi H, Hyung Chang J, Suetsugu S, Tomino Y, Takenawa T, Faul C, Mundel P: Synaptopodin protects against proteinuria by disrupting Cdc42: IRSp53:Mena signaling complexes in kidney podocytes. *Am J Pathol* 171: 415–427, 2007
44. Winn MP, Conlon PJ, Lynn KL, Howell DN, Slotterbeck BD, Smith AH, Graham FL, Bembe M, Quarles LD, Pericak-Vance MA, Vance JM: Linkage of a gene causing familial focal segmental glomerulosclerosis to chromosome 11 and further evidence of genetic heterogeneity. *Genomics* 58: 113–120, 1999
45. O'Connell JR, Weeks DE: The VITESSE algorithm for rapid exact multilocus linkage analysis via genotype set-recoding and fuzzy inheritance. *Nat Genet* 11: 402–408, 1995
46. Terwilliger JD, Speer M, Ott J: Chromosome-based method for rapid computer simulation in human genetic linkage analysis. *Genet Epidemiol* 10: 217–224, 1993
47. Pericak-Vance MA: Analysis of genetic linkage data for Mendelian traits. *Curr Protoc Hum Genet* Chapter 1: Unit 1.4, 2001
48. Westerfield M: *The Zebrafish Book: A Guide for the Laboratory Use of Zebrafish (Brachydanio rerio)*, Eugene, OR, University of Oregon Press, 1993

This article contains supplemental material online at <http://jasn.asnjournals.org/lookup/suppl/doi:10.1681/ASN.2013101053/-DCSupplemental>.